Influence of obstacle-produced turbulence on development of premixed flames

YU Lixin (余立新), SUN Wenchao (孙文超) & WU Chengkang (吴承康)

Institute of Mechanics, Chinese Academy of Sciences, Beijing 100080, China
Correspondence should be addressed to Yu Lixin (email: ylxin@imech.ac.cn)

Received September 24, 2001

Abstract An investigation into influence of obstructions on premixed flame propagation has been carried out in a semi-open tube. It is found that there exists flame acceleration and rising overpressure along the path of flame due to obstacles. According to the magnitude of flame speeds, the propagation of flame in the tube can be classified into three regimes: the quenching, the choking and the detonation regimes. In premixed flames near the flammability limits, the flame is observed first to accelerate and then to quench itself after propagating past a certain number of obstacles. In the choking regime, the maximum flame speeds are somewhat below the combustion product sound speeds, and insensitive to the blockage ratio. In the more sensitive mixtures, the transition to detonation (DDT) occurs when the equivalence ratio increases. The transition is not observed for the less sensitive mixtures. The dependence of overpressure on blockage ratio is not monotonous. Furthermore, a numerical study of flame acceleration and overpressure with the unsteady compressible flow model is performed, and the agreement between the simulation and measurements is good.

Keywords: **equivalence ratio, obstructions, flame acceleration, overpressure, compressible flow mode.**

The study of flame propagation in the tube with obstructions was pioneered by Chapman and Wheeler in 1926. From then on, flame acceleration with turbulence-producing obstacles have been observed by various authors. For example, in tubes open at one end and filled with repeated obstacles, flame speeds greater than 500m/s have been recorded in the relatively insentive mixture of stoichiometric methane and air[1]. Turbulent flame acceleration in closed tubes with several kinds of fuels including H_2, C_2H_2, C_2H_4, CH_4 and C_3H_8 has been carried out by Lee et al.[2—6]. Their results demonstrated that for sensitive mixture such as H_2-air or C_2H_2-air, transition from deflagration to detonation can be observed under certain conditions. However, the experimental data of flame propagation in open tubes are insufficient for various fuels. There is no lack of applications of vented vessel in reality, for instance, a new type of ash-cleaning facility widely used in energy power system is a semi-open system burning gaseous fuels[7]. From a practical point of view, it is of importance to explore the mechanism of unsteady state flame acceleration in the semi-open tube.

In a closed vessel, irrespective of the different possible modes of combustion (deflagration, detonation, etc.), the final equilibrium overpressure increases are more or less the same, corresponding to the constant volume explosion pressure Δp_{cv} which is the property of fuel-air mixture. But for explosions in vented vessel, there is no equilibrium overpressure. The transient pressure rise depends on the vessel geometry, vent area, and burning velocity of mixture. Laminar burning velocities depend on the transport and chemical-kinetics properties of the gas mixture and are typ-

ically less than 1m/s for most stoichiometric hydrocarbon-air mixtures. However, propagation of flame is intrinsically unstable in tubes or channels filled with obstacles, and the rate of burning is strongly influenced by the gas-dynamic flow structure in the unburned gases because of the coupling between the combustion process and the flow ahead. In the present paper, the influence of turbulence on flame propagation in a semi-open tube is studied by changing the configurations of obstacles, the numerical simulations of the development of flame speeds and transient overpressure are performed using the unsteady compressible flow model, and the predicted values are compared with measuremental data.

1 Experimental details

As shown in fig. 1, the flame tube used in the experiments was a semi-open obstructed tube which had a 80 mm inner diameter and was 5 m long. Circular orifice plates spaced 200 mm apart with blockage ratios of $BR = 0.212$, 0.315, 0.438, 0.609 and 0.75 were used as flow obstructives. The blockage ratio is defined as $BR = 1 - (d/D)^2$ where d and D denote orifice and tube inner diameter, respectively. The fuels include H_2, $C - 2H_2$, water gas ($58.5\%H_2$, $30\%CH_4$, $5.4\%N_2$ and $6.1\%CO$), and CH_4.

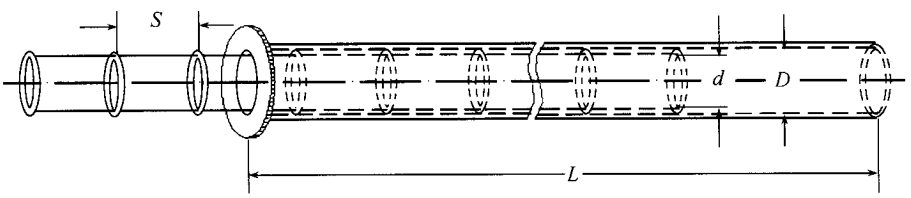

Fig. 1. Schematic diagram of the flame tube and obstacle arrays.

When the tube was fully filled with a premixed gas mixture, the inlet valve was closed, and ignition was initiated by an electrical spark. Now the initial flame was formed. The flame accelerated through the tube from the closed end to the open end due to the turbulence produced by the obstacles. In order to monitor the development of flame speeds and overpressure, ionization probes and pressure transducers were installed at different positions along the tube. When the flame passed, the signals were recorded on a 8 channel high speed digital recorder with top sampling frequency 400 kHz, so that the flame speeds and transient pressure in the tube could be measured.

2 Results and discussion

In the paper, the equivalence ratio is defined as Φ = fuel to air ratio/stoichiometric ratio.

The results of the present study indicated that, according to the magnitude of final quasi-steady state flame speeds, the propagation of flame in the tube can be classified into three regimes due to flame acceleration by turbulence. The quasi-steady state flame speeds depend not only on the fuel and mixture composition, but also on the obstacle configuration (i.e. orifice inner diameter, blockage ratio and obstacle spacing). One propagation regime is typically separated from another by an abrupt jump in the magnitude of the flame velocity. In premixed flames near the

flammability limits, the flame speeds are very low and the flame fails to propagate along the tube and quenches itself because of pressure losses across the obstacles. This is referred to as "the quenching regime". Thibault et al.[8] showed that there exists a critical orifice diameter below which the flame cannot pass forward. This critical orifice diameter was found to depend on the pressure ratio across the orifice plate, the mixture composition and initial conditions. In the following figures, zero terminal velocity is used to represent the quenching regime. When the flame propagation transits from quenching to chocking regime, the transition of flame speed appears, and the flame speed corresponds roughly to the sound speeds of combustion products. The second transition from deflagration to detonation is observed when equivalence ratio increases, and the flame speeds are greater than 1000 m/s.

2.1 Influence of obstacles on flame propagation in the tube

2.1.1 Flame acceleration in the tube. The variation of the flame speed with distance along the flame tube (blockage ratio $BR = 0.438$) is shown in fig. 2 for different equivalence ratios. Owing to the positive feedback mechanism between burning rate of flame and gas-dynamic flow structure, and combining effect of wall friction and heat release, the flame continuously accelerates and eventually reaches a final quasi-steady state, and the maximum flame speed is obtained. A higher equivalence ratio gives rise to a higher accelerating rate, making the distance to quasi-steady state much shorter. For instance, as far as hydrogen-air mixture is concerned, for equivalence ratio $\Phi = 0.69$, the flame speed reaches the maximum value at $x/L = 0.36$, corresponding to 1786 m/s, but for $\Phi = 0.58$, the flame gets to quasi-steady state only at $x/L = 0.48$, and the maximum flame speed is just about 800 m/s. In addition, the flame accelerating rate depends on the fuel. For the same obstacle configuration and blockage ratio ($BR = 0.438$, $\Phi = 0.58$), the distances to quasi-steady state for hydrogen, water gas and methane are $x = 0.48$, 0.64, 0.8 L, respectively, and the maximum flame speed corresponds to 800, 450, and 200 m/s, respectively.

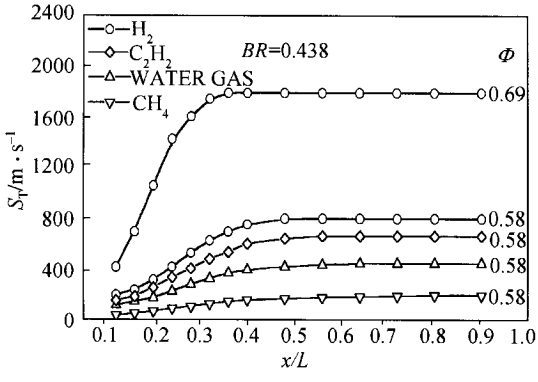

Fig. 2. Variation of flame speed along the tube for different fuels ($BR = 0.438$).

2.1.2 The different regimes of flame propagation. When flame propagates along the obstructed tube, for sensitive gases such as hydrogen or acetylene, the propagation of flame can be classified into three regimes according to the magnitude of the maximum flame speeds. In the quenching regime, although the initial flame is formed, the flame eventually extinguishes itself after propagating across a little distance and cannot go forward any more because of turbulence induced by obstacles. If the equivalence ratio is raised, the flame accelerates continuously and no longer quenches, the final flame speed is close to the sound speed of burnt combustion products. When this happens, the flame propagation gets into the choking regime. With the increasing equiva-

lence ratio, the second sudden jump in the flame speed occurs, transition from deflagration to detonation is observed, and the flame speed approaches the normal C-J value. However, for relatively insensitive gases, such as water gas or methane, there is no transition to detonation in the present experiment, as shown in fig. 3.

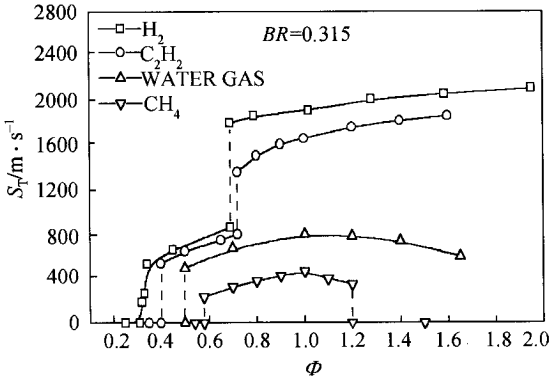

Fig. 3. The maximum flame speeds vs. fuel and equivalence ratio (BR = 0.315).

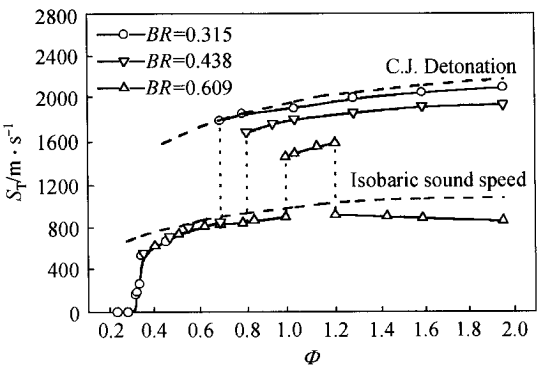

Fig. 4. Influence of blockage ratio on the regime of flame propagation (hydrogen-air).

Fig. 4 shows the influence of blockage ratio on the regime of hydrogen-air flame propagation. Although the lean limit of hydrogen-air is $\Phi \approx 0.1$, there is no flame signal for $\Phi \leqslant 0.32$ due to the strong turbulence by obstacles. It is indicated that the flame quenches itself soon after ignition. In the choking regime, according to compressible flow theory, friction and heat addition will eventually drive the flow to move at the sound speed. In fact, the flame speed is lower than the sound speed of the combustion products computed on the basis of an isobaric combustion process due to the momentum deficit and heat losses induced by the blockage effect of obstacles. The measured value is about 100m/s below the isobaric sound speed curve and follows the trend of the curve in this way as a function of mixture composition. The flame speed is also insensitive to the blockage ratio, which is consistent with the flow behavior of the choked conditions. For detonative combustion, a decrease in maximum flame speed is found with increasing blockage ratio due to higher pressure loss across the obstacle. It is found that at $\Phi = 1.02$, the maximum flame speeds are 1900, 1800 and 1480 m/s for different blockages of 0.315, 0.438 and 0.609, respectively. The velocity deficit is as high as 420 m/s. The range of detonation also reduces with the increase in blockage. It is shown that at $BR = 0.609$, transition to detonation is suppressed. Thus it is reasonable to expect that there exists a critical blockage ratio above which transition to detonation fails to occur for any given mixture composition.

2.2 Influence of obstacles on overpressure in the tube

2.2.1 Overpressure development in the tube.

When flame accelerates in the tube, it pushes forward and compresses the unburnt gas resulting in a rise in overpressure, as shown in fig. 5(a).

In the condition of $BR = 0.438$ and $\Phi = 0.58$, the maximum flame speed of methane-air is only 200 m/s (fig. 2), which is far lower than the corresponding sound speed ~ 800m/s. In

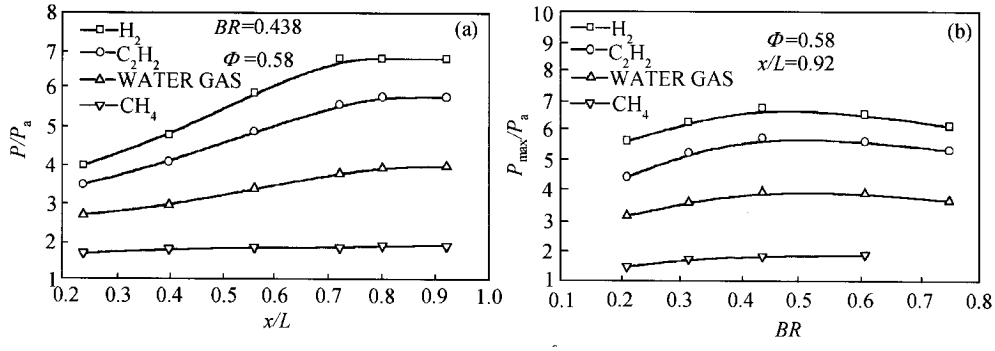

Fig. 5. Influence of obstacles on overpressure in the tube (P_a is atmosphere). (a) Maximum overpressure of 4 kinds of mixtures at various positions in the tube with BR = 0.438 and Φ = 0.58; (b) variation of maximum overpressure with blockage ratio for various mixtures.

this case, the flow in the tube can be considered as incompressible, so that the overpressures along the tube are more or less the same. However, the trend of development of overpressure is very similar to that of flame acceleration for hydrogen and acetylene. Fig. 4 shows that the flame speeds are close to the sound speed within the choking regime; thus the influence of flow compressibility on pressure fluctuation cannot be neglected, and a one-way characteristic appears in the pressure transmission. With the movement of pressure wave, the overpressure goes up continuously and finally reaches a quasi-steady state.

2.2.2 Influence of obstacles on the maximum overpressure. Fig. 5(b) illustrates the variation of the maximum overpressure with blockage ratio. The influence of blockage ratio on the maximum overpressure changes with different fuels (fig. 5(b)). An increase in overpressure with increasing blockage ratio is observed in the case of methane. Nevertheless, there exists similar behavior for other three fuels, i.e. the maximum overpressure goes up with the increasing blockage ratio when blockage ratio is less than 0.5, but when of blockage is larger than 0.5, the maximum overpressure goes down with rising blockage ratio. The overpressure reaches an extreme top value at about blockage ratio of 0.5.

3 Numerical simulation

From the above discussion, it can be concluded that under appropriate conditions of equivalence ratio and obstacle configuration, transition to detonation occurs. When this happens, the combustion wave is accompanied by shock wave in the tube. As a result, the propagation mechanism of detonation is so different from that of deflagration that they cannot be studied using a unified theory. Thus the effect of shock wave on combustion process is not involved in the following numerical study, and prediction is limited to the development of flame in the condition of subsonic deflagration.

3.1 Turbulence model

In the present paper, the numerical study of flame acceleration and development of overpressure due to turbulence-producing obstacles was performed using the unsteady compressible flow

model. The calculation was limited to the two-dimensional axisymmetric condition. Owing to the high Mach number of turbulent flow in the flame propagation, the influence of turbulence Mach number on viscosity-dissipation and pressure-dilatation had been considered on the basis of previous work[9], and the correction of the existing compressible k-ε turbulent model was performed.

3.1.1 The compressible correction of k-ε turbulent model. The equation of turbulent kinetic energy k is expressed as

$$\frac{\partial(\bar{\rho}k)}{\partial t} + \frac{\partial(\bar{\rho}\tilde{u}_j k)}{\partial x_j} = D_{ij} + P_{ij} + \Pi_{ij} - \varepsilon_{ij} - \overline{\frac{\rho' u_i''}{\bar{\rho}}}\frac{\partial \bar{p}}{\partial x_j}, \tag{1}$$

where the detailed expressions of the various terms on the right-hand side are as follows:

The stress-divergence

$$D_{ij} = \frac{\partial}{\partial x_j}\left[\frac{1}{2}\overline{\rho u_i'' u_i'' u_j''} + (\overline{p' u_i''})\delta_{ij} - \overline{\tau'_{ij} u_i''}\right], \tag{2}$$

which includes turbulent kinetic energy divergence $\frac{1}{2}\overline{\rho u_i'' u_i'' u_j''}$, pressure-divergence $(\overline{p' u_i''})\delta_{ij}$, and viscosity-divergence $-\overline{\tau'_{ij} u_i''}$.

The production of turbulent kinetic energy

$$P_{ij} = -\overline{\rho u_i'' u_j''}\frac{\partial \tilde{u}_i}{\partial x_j}. \tag{3}$$

The pressure-dilatation

$$\Pi_{ij} = \overline{p'\frac{\partial u_i''}{\partial x_j}}. \tag{4}$$

The turbulent kinetic energy dissipation

$$\varepsilon_{ij} = \bar{\rho}\varepsilon = \overline{\tau'_{ij}\frac{\partial u_i''}{\partial x_j}}. \tag{5}$$

Using gradient modeling, we have

$$-\frac{1}{2}\overline{\rho u_i'' u_i'' u_j''} - \overline{p' u_i''}\delta_{ij} = \frac{\mu_t}{\sigma_k}\frac{\partial k}{\partial x_j}, \quad -\overline{\rho' u_i''} = \frac{\mu_t}{\bar{\rho}}\frac{\partial \bar{\rho}}{\partial x_i}.$$

From the hypothesis of Boussinesq, we obtain

$$-\overline{\rho u_i'' u_j''} = \mu_t\left(\frac{\partial \tilde{u}_i}{\partial x_j} + \frac{\partial \tilde{u}_j}{\partial x_i}\right) - \frac{2}{3}\left(\bar{\rho}k + \mu_t\frac{\partial \tilde{u}_k}{\partial x_k}\right).$$

The fluctuation-dilatation $d' = \dfrac{\partial u_i''}{\partial x_j}$ is included in the pressure-dilatation Π_{ij} and the turbulent kinetic energy dissipation ε_{ij}. The compressibility of flow is chiefly reflected as the density fluctuation which is related to the fluctuation-dilatation d'.

For high Reynolds number compressible turbulence, in the case of homogeneity, the turbulent kinetic energy dissipation can be expressed as[10]

$$\bar{\rho}\varepsilon = \mu\left(\overline{\omega_i\omega_i} + \frac{4}{3}\mu\,\overline{d'd'}\right) = \bar{\rho}\varepsilon_s + \bar{\rho}\varepsilon_d, \tag{6}$$

where $\omega_i = \nabla \times u_i''$ and $d' = \nabla \cdot u_i''$, $\bar{\rho}\varepsilon_s = \mu\,\overline{\omega_i\omega_i}$ is the incompressible dissipation, and $\bar{\rho}\varepsilon_d = \frac{4}{3}$

$\mu\ \overline{d'd'}$ the compressible dilatation dissipation.

According to the discussion of previous works[11—13], a plausible parametric relationship is

$$\varepsilon_d = 0.15 H(M_t)\varepsilon_s, \tag{7}$$

$$H(M_t) = \begin{cases} (M_t^2 - M_{t0}^2), & M_t \geqslant M_{t0}, \\ 0, & M_t < M_{t0}, \end{cases} \tag{8}$$

where the turbulence Mach number $M_t = \sqrt{2k}/c$, c is the sound speed, and M_{t0} equals 0.25.

The pressure-dilatation $\overline{p'd'}$ can be derived from the following relationship[14,15]:

$$\overline{p'd'} = 0.2\ M_t^2 \bar{\rho}\ \varepsilon_s - 0.4\ M_t^2 \bar{\tau}_{ij} \frac{\partial \tilde{u}_i}{\partial x_j}. \tag{9}$$

In all the equations above, a signal superscript $'$ represents fluctuation with respect to the Reynolds average, while a double superscript $''$ signifies fluctuation with respect to the Favre average.

3.1.2 Control equations. The modified control equations are as follows:

$$\frac{\partial \bar{\rho}}{\partial t} + \frac{\partial (\bar{\rho}\tilde{u}_j)}{\partial x_j} = 0, \tag{10}$$

$$\frac{\partial (\bar{\rho}\tilde{u}_i)}{\partial t} + \frac{\partial (\bar{\rho}\tilde{u}_i\tilde{u}_j)}{\partial x_j} = -\frac{\partial \bar{p}}{\partial x_i} + \frac{\partial}{\partial x_j}(\bar{\tau}_{ij} - \bar{\sigma}_{ij}), \tag{11}$$

$$\frac{\partial (\bar{\rho}\tilde{h})}{\partial t} + \frac{\partial (\bar{\rho}\tilde{u}_j\tilde{h})}{\partial x_j} = \frac{\partial}{\partial x_j}\left[\left(\frac{\mu}{P_r} + \frac{\mu_t}{\sigma_h}\right)\frac{\partial \tilde{h}}{\partial x_j}\right] + \bar{\tau}_{ij}\frac{\partial \tilde{u}_i}{\partial x_j} + \bar{\rho}\varepsilon + \frac{\partial \bar{p}}{\partial t} + \tilde{u}_j\frac{\partial \bar{p}}{\partial x_j} + \frac{\mu_t}{\bar{\rho}^2}\frac{\partial \bar{\rho}}{\partial x_j}\frac{\partial \bar{p}}{\partial x_j}, \tag{12}$$

$$\frac{\partial (\bar{\rho}\tilde{Y}_f)}{\partial t} + \frac{\partial (\bar{\rho}\tilde{u}_j\tilde{Y}_f)}{\partial x_j} = \frac{\partial}{\partial x_j}\left[\left(\mu + \frac{\mu_t}{\sigma_Y}\right)\frac{\partial \tilde{Y}_f}{\partial x_j}\right] + \bar{R}_{fu}, \tag{13}$$

$$\frac{\partial (\bar{\rho}f)}{\partial t} + \frac{\partial (\bar{\rho}\tilde{u}_j f)}{\partial x_j} = \frac{\partial}{\partial x_j}\left[\left(\mu + \frac{\mu_t}{\sigma_f}\right)\frac{\partial f}{\partial x_j}\right], \tag{14}$$

$$\frac{\partial (\bar{\rho}k)}{\partial t} + \frac{\partial (\bar{\rho}\tilde{u}_j k)}{\partial x_j} = \frac{\partial}{\partial x_j}\left[\left(\mu + \frac{\mu_t}{\sigma_k}\right)\frac{\partial k}{\partial x_j}\right] - \bar{\sigma}_{ij}\frac{\partial \tilde{u}_i}{\partial x_j} \cdot F(M_t) - \frac{\mu_t}{\bar{\rho}^2}\frac{\partial \bar{\rho}}{\partial x_j}\frac{\partial \bar{p}}{\partial x_j} - \bar{\rho}\varepsilon \cdot G(M_t), \tag{15}$$

$$\frac{\partial (\bar{\rho}\varepsilon)}{\partial t} + \frac{\partial (\bar{\rho}\tilde{u}_j\varepsilon)}{\partial x_j} = \frac{\partial}{\partial x_j}\left[\left(\mu + \frac{\mu_t}{\sigma_\varepsilon}\right)\frac{\partial \varepsilon}{\partial x_j}\right] - C_1\frac{\varepsilon}{k}\left(\bar{\sigma}_{ij}\frac{\partial \tilde{u}_i}{\partial x_j} + \frac{\mu_t}{\bar{\rho}^2}\frac{\partial \bar{\rho}}{\partial x_j}\frac{\partial \bar{p}}{\partial x_j}\right) - C_2\bar{\rho}\frac{\varepsilon^2}{k}, \tag{16}$$

where

$$\tilde{h} = C_p\tilde{T} + \tilde{Y}_f Q_f, \tag{17}$$

$$f = \tilde{Y}_f - \frac{\tilde{Y}_{O_2}}{\beta}, \tag{18}$$

$$\bar{\tau}_{ij} = \mu\left(\frac{\partial \tilde{u}_i}{\partial x_j} + \frac{\partial \tilde{u}_j}{\partial x_i}\right) - \frac{2}{3}\mu\frac{\partial \tilde{u}_k}{\partial x_k}\delta_{ij}, \tag{19}$$

$$\bar{\sigma}_{ij} = -\mu_t\left(\frac{\partial \tilde{u}_i}{\partial x_j} + \frac{\partial \tilde{u}_j}{\partial x_i}\right) + \frac{2}{3}\delta_{ij}\left(\bar{\rho}k + \mu_t\frac{\partial \tilde{u}_k}{\partial x_k}\right), \tag{20}$$

$$\mu_t = C_\mu \bar{\rho}\frac{k^2}{\varepsilon}, \tag{21}$$

$$F(M_t) = 1 - 0.4\,M_t, \tag{22}$$

$$G(M_t) = \begin{cases} 1 + 1.5(M_t^2 - M_{t0}^2) - 0.2M_t^2, & M_t \geqslant M_{t0}, \\ 1 - 0.2M_t^2, & M_t < M_{t0}. \end{cases} \tag{23}$$

$\tilde{Y}_f$ is mass fraction of fuel, $\tilde{Y}_{O_2}$ mass fraction of oxygen, f mixture fraction, Q_f heat of reaction per unit mass, and β is a measure coefficient where the combustion equation based on the mass is assumed to be $\{F\} + \beta\{O_2\} \rightarrow (1 + \beta)\{P\}$. $F(M_t)$ and $G(M_t)$ are given functions. The symbol ~ signifies Farve-averaged quantities, and overbar "—" designates Reynolds average. The constants used in the model are shown in table 1.

Table 1 The Model constants

C_μ	C_1	C_2	σ_h	σ_Y	σ_f	σ_k	σ_ε
0.09	1.44	1.92	0.7	0.7	0.7	1.0	1.3

3.2 Combustion model

The source term related with rate of combustion is included in the species conservation. The time mean rate of combustion is treated by Eddy-Break-Up model as the following relationship[16]:

$$\bar{R}_{fu} = -C_{\mathrm{EBU}}\bar{\rho}\frac{\varepsilon}{k}\tilde{Y}_{\lim}, \tag{24}$$

where $\tilde{Y}_{\min} = \min[\tilde{Y}_f, \tilde{Y}_{O_2}/\beta, \tilde{Y}_p]$, $C_{\mathrm{EBU}} = 4.0$.

3.3 Domain of calculation

The calculation domain is divided into $502 \times 22 = 11044$ grid points in the x-direction and the radial direction, respectively (fig. 6). The staggered grid has been used in the calculation. In the initial condition, the tube was fully filled with premixed combustible mixture, and ignition was initiated by a planar source at the closed end. The flow was treated as being in the turbulent regime from the start $t = 0$ and no attempt was made to model the laminar to turbulent flow transition. We say that the ignition was accomplished when 20 percent of fuel at the closed end of the tube was burnt. The reaction rate and effective viscosity were dependent on the initial value of the dissipation rate ε_0.

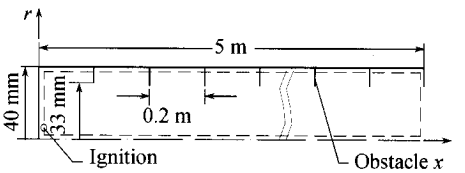

Fig. 6. Domain of calculation.

3.4 Boundary conditions

(1) At axial center line: The axisymmetric condition is adopted. This means that the axial velocities, turbulent kinetic energy and radial gradient of dissipation rate of turbulent kinetic energy are set at zero, and radial velocities are set at zero, too.

(2) At wall: The wall function is adopted.

(3) At outlet: It is assumed that the first derivatives of normal velocities at the outlet points are constant. According to the total mass conservation principle, the velocities at the outlet points can be obtained from the contribution of velocities of inner points.

(4) At obstacles: It is presumed that the thickness of obstacles is negligible, the flow viscosity at obstacles is infinite, and the velocities at the boundary are set at zero.

3.5 Computational results

The computed flame contours of acetylene-air at different time are depicted in fig. 7 with equivalence ratio 0.58 and blockage ratio 0.315. The flame becomes deformed when it passes through the obstacles. With the flame moving forward to the outlet, the turbulence gets stronger because of obstacles, and the flame is so distorted that the leading front at the axial centerline accelerates continuously, which is consistent with the measurement of ref. [17].

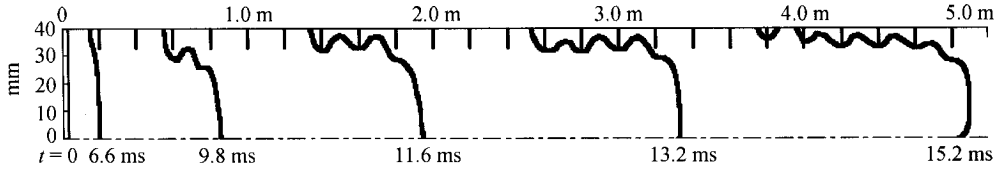

Fig. 7. The computed flame contours at the different time.

The comparison of predicted maximum flame speeds and maximum overpressure in the tube with the experimental data in fig. 8 shows good agreement. It is reasonable to use the above turbulent flow model to analyze the development of premixed flame in the obstructed tube. However, neither prediction of transition to detonation nor that of the composition range of flame quenching can be made by the present model, in that the effect of shock wave on the combustion or chemical kinetic effects at quenching are not involved in the model.

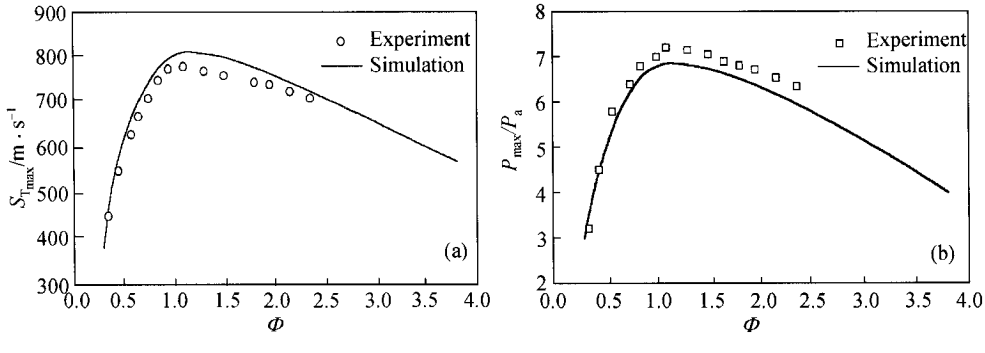

Fig. 8. A comparison of calculated values with experimental data for acetylene-air premixed flame. (a) The maximum flame speed vs. equivalence ratio; (b) the maximum overpressure vs. equivalence ratio.

4 Conclusions

The influence of turbulence produced by obstacles on flame propagation in a semi-open tube has been studied with 4 kinds of fuels. It can be concluded that there exist three distinct regimes

of flame propagation in the obstacle-filled tube. In premixed flames near the flammability limits, the flame extinguishes itself after propagating some distance. This is referred to as the quenching regime. When the equivalence ratio is so high that quenching does not occur, the flame accelerates continuously and the overpressure goes up along the tube, ultimately reaching a quasi-steady state. This regime is called the choking regime. With the increasing equivalence ratio, the transition from deflagration to detonation is observed for sensitive mixtures, the sudden jump in the flame speed occurs from one regime to another. However, there exists no transition to detonation for relatively insensitive mixtures in the present condition.

In the choking regime, the maximum flame speed is insensitive to the blockage ratio, and somewhat below the sound speed of burnt products. Nevertheless, in the detonation regime, the maximum flame speed decreases with the increasing blockage ratio due to the severe momentum losses induced by the blockage effect of the obstacles, and at the same time, the detonative range is observed to become narrower. The effect of blockage ratio on overpressure is not monotonous, and the overpressure reaches its maximum at about blockage ratio of $BR = 0.5$.

By the correction of viscosity-dissipation and pressure-dilatation, the modified k-ε two-dimension turbulent model has been used to predict the flame acceleration and the development of overpressure in the tube, the calculated overpressure and flame speeds are in good agreement with experimental data. However, a great deal of attempts must be made to predict the transition to detonation.

Acknowledgements This work was supported by the National Key Fundamental Research and Development Program of China (Grant No. G1999022305).

References

1. Chan, C., Lee, J. H. S., Moen, I. O. et al., Turbulent flame acceleration and pressure development in tubes, in Proceedings of the First Specialist Meeting of the Combustion Institute, Bordeaux, France, July, 1981: 479—487.
2. Moen, I. O., Donato, M., Knystautas, R. et al., Flame acceleration due to turbulence produced by obstacles, Combustion and Flame, 1980, 39: 21—32.
3. Moen, I. O., Lee, J. H. S., Hjertager, B. H. et al., Pressure development due to turbulent flame propagation in large-scale methane-air explosions, Combustion and Flame, 1982, 47: 31—52.
4. Lee, J. H., Knystautas, R., Freiman, A., High speed turbulent deflagrations and transition to detonation in H_2-Air mixtures, Combustion and Flame, 1984, 56: 227—239.
5. Hjertager, B. H., Fuher, K., Parker, S. J. et al., Flame acceleration of propane-air in a large-scale obstructed tube, dynamics of shock waves, Explosions and Detonations, 1984, 94: 504—522.
6. Lee, J. H., Knystautas, R., Chan, C. K., Turbulent flame propagation in obstacle-filled tubes, in 20th Symposium (International) on Combustion, Pittsburg: the Combustion Institute, 1984, 1663—1672.
7. Yu Lixin, Sun Wenchao, Wu Chengkang, Study on application of gas-pulse ash-cleaning technology, Journal of Combustion Science and Technology (in Chinese), 2001, 7(3): 223—227.
8. Thibault, P., Liu, Y. K., Chan, C. et al., Transmission of an explosion through an orifice, in 19th Symposium (International) on Combustion, Pittsburg: the Combustion Institute, 1982, 599—606.
9. Hjertager, B. H., Simulation of transient compressible turbulent reactive flows, Combustion and Technology, 1982, 27: 159—170.
10. Sarkar, S., Erlebacher, G., Huaasini, M. Y. et al., The analysis and modeling of dilatational terms in compressible turbulence, ICASE Report, 1989, 89—79.

11. Zeman, O., Dilatation dissipation: The concept and application in modeling compressible mixing layers, Phys. Fluids A, 1990, 2(2): 178—188.
12. Sarkar, S., The pressure-dilatation correlation in compressible flows, Phys. Fluids A, 1992, 4(12): 2674—2682.
13. Wilcox, D. C., Progress in hypersonic turbulence modeling, AIAA-91-1785, June, 1991.
14. Liang Dewang, Wang Guoqing, Modification of two-equation turbulence models with compressibility and its application, Acta Aerodynamic Sinica (in Chinese), 2000, 18(1): 98—104.
15. Haidinger, F. A., Friedrich, R., Numerical simulation of strong shock/turbulent boundary layer interactions using a Reynolds stress model, Z. Flugwiss. Weltraumforsch, 1995, 19: 10—18.
16. Magnussen, B. F., Hjertager, B. H., On mathematical modelling of turbulent combustion with special emphasis on soot formation and combustion, in 16th Symposium (International) on Combustion, Pittsburg: the Combustion Institute, 1976, 719—729.
17. Fan Weijun, Study on combustion and ash-cleaning process of gas-pulse ash-cleaning technology (in Chinese), Doctoral Dissertation, Institute of Mechanics, Chinese Academy of Sciences, 1999.